Published online 15 March 2017

Nucleic Acids Research, 2017, Vol. 45, No. 9 ***5269–5284***
doi: 10.1093/nar/gkx176

Rgf1p (Rho1p GEF) is required for double-strand break repair in fission yeast

Elvira Manjón, Tomás Edreira, Sofía Muñoz and Yolanda Sánchez*

Instituto de Biología Funcional y Genómica, CSIC. Departamento de Microbiología y Genética, Universidad de Salamanca. C/ Zacarías González, s/n. Salamanca, Spain

Received October 20, 2016; Revised March 02, 2017; Editorial Decision March 03, 2017; Accepted March 07, 2017

ABSTRACT

Rho GTPases are conserved molecules that control cytoskeletal dynamics. These functions are expedited by Rho GEFs that stimulate the release of GDP to enable GTP binding, thereby allowing Rho proteins to initiate intracellular signaling. How Rho GEFs and Rho GTPases protect cells from DNA damage is unknown. Here, we explore the extreme sensitivity of a deletion mutation in the Rho1p exchange factor Rgf1p to the DNA break/inducing antibiotic phleomycin (Phl). The Rgf1p mutant cells are defective in reentry into the cell cycle following the induction of severe DNA damage. This phenotype correlates with the inability of *rgf1*Δ cells to efficiently repair fragmented chromosomes after Phl treatment. Consistent with this observation Rad11p (ssDNA binding protein, RPA), Rad52p, Rad54p and Rad51p, which facilitate strand invasion in the process of homology-directed repair (HDR), are permanently stacked in Phl-induced foci in *rgf1*Δ cells. These phenotypes are phenocopied by genetic inhibition of Rho1p. Our data provide evidence that Rgf1p/Rho1p activity positively controls a repair function that confers resistance against the anti-cancer drug Phl.

INTRODUCTION

Rho GTPases are key regulators of the actin cytoskeleton dynamics. Moreover, they also regulate diverse cellular functions including cell cycle, gene expression, vesicle trafficking and cell polarity (1–3). Most Rho GTPases switch between an active GTP-bound conformation, which interacts with downstream effectors, and an inactive GDP-bound conformation. Exchange of GDP for GTP induces activation, and this is catalyzed by guanine nucleotide exchange factors (GEFs) (4). Besides their classical role as membrane-bound signal transducing molecules, it has recently been shown that Rho GEFs, Rho GTPases and downstream components are found in the nucleus, suggesting that Rho-related signaling processes may also take place in this cellular compartment (5,6). Indeed, RhoA and RhoB are DNA damage-inducible genes, and their abundance determines cell fate after DNA damage (7,8). Nuclear Rho GEFs, Net1p and Ect2p, regulate RhoA- and RhoB-mediated cell dead after DNA damage (9–11). Despite the knowledge accumulated, the role of Rho proteins in DNA repair is not well understood.

DNA double-strand breaks (DSBs) are among the most severe lesions, and their inefficient repair can initiate genomic instability, ultimately leading to cancer (12). In consequence, cells have developed complex signaling networks that sense DSBs, arrest the cell cycle, and activate repair pathways (13–15). The mechanism that a cell uses to repair a DSB is mainly determined during certain cell cycle stages: non homologous end joining (NHEJ) in G1 and homologous recombination (HR) in S and G2, when the sister chromatid is accessible for use as a template for repair (16,17). In NHEJ, the DSB ends are blocked from 5′ end resection and the Ku70-Ku80 complex promotes direct ligation of the DSB ends, but in an error-prone manner. In contrast, HR is largely error free and is initiated when the DSB is resected by nucleases and helicases, generating 3′ single-stranded DNA (ssDNA) overhangs onto which the Rad51p recombinase assembles as a nucleoprotein filament. This structure can invade homologous duplex DNA, which is used as a template for DNA synthesis.

In fission yeast, Rad51p, Rad52p and Rad54p are responsible for catalyzing HR (18). These factors, when fused to a fluorescent protein, form microscopically discernible repair centers at the sites of damage in both fission (19) and budding yeast (20). Beside the recruitment of these repair proteins, the resection of DNA at a cut site leads to activation of the ATR kinase complex Rad3p and, in turn, the downstream checkpoint kinases Cds1p and Chk1p. The DNA damage checkpoint pathway blocks cell cycle progression until DNA repair is completed and promotes extensive resection and nucleotide synthesis to facilitate homologous recombination repair (21,22). In spite of our knowledge, the mechanisms by which DSBs encounter potential donor sequences (23–25) and the connections between repair cen-

*To whom correspondence should be addressed. Tel: +34 923 29 48 82; Fax: +34 923 22 48 76; Email: ysm@usal.es
Present address: Sofia Muñoz, The Francis Crick Institute, Lincoln's Inn Fields Laboratory, London WC2A 3LY, UK.

ters and cytoskeletal proteins have yet to be fully elucidated (26,27).

Fission yeast Rho1p is a functional homologue of human RhoAp and budding yeast Rho1p (28). Rho1p regulates cell integrity and polarized secretion; depletion of its activity in growing cells causes cell lysis, the cells shrink and die in a kind of 'apoptosis' that is accompanied by the disappearance of polymerized actin (29,30). Rho1p activity is regulated by three GEFs, Rgf1p, Rgf2p and Rgf3p, that catalyze the exchange from GDP to GTP, rendering the GTPase in an active state (31–35). Rho1p-GTP binds and activates the protein kinases of the PKC family, Pck1p and Pck2p (36), which function upstream of the MAPK module (Mkh1p, Skh1p/Pek1p and Pmk1p/Spm1p) of the cell integrity signaling pathway (CIP) (37–40). Among the Rho1p-GEFs, Rgf1p is the most prominent, and activates Rho1p during polarized growth. Rgf1p is required for the actin reorganization necessary for cells to change from monopolar to bipolar growth during NETO (New End Take Off) (30,32). Recently, we found that Rgf1p is also required for tolerance to chronic replication stress. The protein shuttles in and out of the nucleus in the absence of DNA damage, and is accumulated within the cell´s nucleus in response to replicative stress (41).

Here, we observed that elimination of Rgf1p led to extreme sensitivity to the double-strand break (DSB)-inducing antibiotic, Phleomycin. Rgf1p influences the DNA damage response at two levels: checkpoint inactivation and DSB repair.

MATERIALS AND METHODS

General yeast methods

Standard procedures and media for *S. pombe* genetics were used as previously described (42). Cultures were grown in rich medium containing yeast extract plus supplements (YES), selective medium (MM) supplemented with the appropriate requirements, or sporulation medium (MEA). The strains used are listed in Table 1. HU, CPT, MMS and Phl were added to the medium after autoclaving. We were advised to take special care when using Phl as the medium has to be maintained at 50–55 °C for at least 3 h after autoclaving.

Survival assays

For DNA damage sensitivity assays (chronic exposure), cells were grown in YES (yeast extract, glucose, and supplements) plates for 2 days. Cells were resuspended in water and spotted as serial dilutions (8×10^4 cells in the left row, and then 4×10^4, 2×10^4, 2×10^3, 2×10^2 and 2×10^1 in each subsequent spot) onto YES plates or YES supplemented with the indicated amounts of hydroxyurea (HU), camptothecin (CPT), methyl methanesulfonate (MMS) and phleomycin (Phl). For UV treatment, cells were serially diluted onto YES plates and irradiated using a Stratagene UV source. For IR treatment, cells were irradiated in a Gammacell 1000 Elite irradiator, with a source of 24.8 TBq of Cs-137. For survival of acute exposure to Phl, midlog-phase cells were cultured in YES media containing 10 μg/ml Phl for 6 h. At 0 h, 3000 cells were plated onto YES agar plates in triplicate and at the indicated time-points, the same culture volume was taken, Phl was washed out, and the cells were plated in triplicate. Survival was estimated relative to untreated cells. All survival assays were carried out in triplicate and, unless otherwise stated, recovery was for 5 days at 28°C.

Preparation of lysates and western blot analyses

Strains with the HA-tagged allele of *chk1*$^+$ integrated at the genomic *chk1* locus were used (Table 1). For cell lysate preparation, approximately 20 ml of exponentially growing cells (OD = 0.8) were collected, washed once with cold water, and frozen at –80°C in 100μl of 20%TCA (Trichloroacetic Acid, Panreac). Acid-washed glass beads were added and cell homogenates were prepared in a 'Fast Prep' FP120 device (Savant; Bio101). Extracts were cleared by centrifugation at 3000 rpm for 10 min, and the pellets were resuspended in 50 μl of 2× sample buffer (100 mM HCl–Tris, pH 6.8, 4% SDS, 20% glycerol, 25 mM DTT and 0.4% bromophenol blue), after which 50 μl of Tris Base 2 M [pH 7.5] was added. The solution was vortexed, boiled for 5 min, and centrifuged at 13 000 rpm for 5 min to collect the supernatant (protein extract sample). Proteins were resolved by SDS-PAGE using 10% gels with an acrylamide/bisacrylamide ratio of 99:1, transferred to nitrocellulose membranes, blocked with 5% milk in Tris-buffered saline with 0.03% Tween, and subjected to immunoblotting with the α-HA antibody (Roche).

Phostag

TCA samples from the HA-tagged allele of *cds1*$^+$ integrated at the genomic *cds1* locus, were resolved by SDS-PAGE using 10% gels with an acrylamide/bisacrylamide ratio of 29:1, with 37.5 μM of PhosTag and 75 μM of $(H_2O)_4MnCl_2$ for 4 h at 100 V constant voltage, keeping the electrophoresis tank in ice. Then, the gel was soaked in transfer buffer (25 mM Tris Base, 192 mM glycine and 20% ethanol) containing 1 mM EDTA for 10 min with gentle agitation. The next wash was performed with transfer buffer without EDTA for another 10 min. The transfer conditions included a constant voltage of 320 mA for 100 min on ice, and proteins were detected by immunoblotting with the α-HA antibody (Roche).

Flow cytometry

Cells were fixed in 70% ethanol and then treated with 0.1 mg/ml RNase A in 50 mM sodium citrate for at least 2 h at 37°C to eliminate RNA. Cells were stained with 32 μg/ml propidium iodide, sonicated and analyzed using a FACSCalibur (Becton, Dickinson) device. Data analysis was carried out with Cell Quest software.

Pulsed-field gel electrophoresis (PFGE)

The repair kinetics of DNA DSBs in early log-phase cells treated with 10 μg/ml Phl for 30 min were analyzed by PFGE. Plugs were prepared as described in the manufacture's instruction (CHEF Genomic DNA Plug Kits, Bio-Rad Laboratories, Inc., USA) with the following modifications: 5×10^8 cells were washed twice in 30 ml of CSE

Table 1. *S. pombe* strains used in this work

Strains	Genotypes
EM28	h$^-$ *rgf1::nat, leu1-32, ura4D18*
PG244[b]	h$^-$ *leu1-32, ura4d18*
VT14	h$^-$ *rgf1::his3$^+$, leu1-32, ade6M210, ura4D18, his3d1*
SM306[c]	h$^+$ *rad3::ura4$^+$, ura4D18, leu1-32*
EM656	h$^-$ *rad3::ura4$^+$, rad52:YFP:kan, leu1-32*
SM305[c]	h$^-$ *cds1::ura4$^+$, leu1-32, ura4D18*
SM304[c]	h$^-$ *chk1::ura4$^+$, leu1-32, ura4D18*
SM331	h$^-$ *chk1::ura4$^+$, rgf1::his3$^+$, leu1-32*
EM318	h$^-$ *chk1::ura4$^+$, rad52:YFP:kan, leu1-32*
EM672	h$^-$ *crb2::kanMX6, rad52:YFP:kan, leu1-32, ura4D18*
SM429[a]	h$^-$ *chk1-HA:ura$^+$, leu1-32 ade6-216*
SM435	h$^-$ *rgf1::nat*, *chk1-HA:ura*, leu1-32
SM438[d]	h$^-$ *atb2-GFP:ura4$^+$, Htt1-RFP: kanMX6*, *leu1-32*
SM439	h$^-$ *atb2-GFP:ura4$^+$, Htt1-RFP: kanMX6*, *rgf1::nat, leu1-32*
SM329[c]	h$^-$ *cds1-2HA6His:ura$^+$, leu1-32*
SM55	h$^-$ *rgf1::his3$^+$, leu1-32::rgf1*-DEPΔ*:leu1$^+$, his3d1, ura4D18, ade6M210*
SM63	h$^-$ *rgf1::his3$^+$, leu1-32::rgf1*-NΔ*:leu1$^+$, his3d1, ura4D18, ade6M210*
SM65	h$^-$ *rgf1::his3$^+$, leu1-32::rgf1*-PHΔ*:leu1$^+$, his3d1, ura4D18, ade6M210*
SM128	h$^-$ *rgf1::his3$^+$, leu1-32::rgf1*-CNH1Δ*:leu1$^+$, his3d1, ura4D18, ade6M210*
PG52	h$^-$ *rgf1::his3$^+$, leu1-32:: rgf1$^+$ (PTTR*Δ*):leu1$^+$, his3d1, ura4D18, ade6M210*
EM4	h$^-$ *rgf2::kanMx4, leu1-32, ade6M210, ura4D18, his3d1*
GI1	h$^+$ *ehs2-1* (*rgf3*), *leu1-32*
MS191	h$^-$ *pck1::ura4$^+$, leu1-32, ura4D18*
PG259[b]	h$^+$ *pck2::kanMX6, leu1-32*
PG347[e]	h$^-$ *pmk1::ura4$^+$ ura4D18*
EM312[b]	h$^+$ *rho1-596:nat, ura4D18, leu1-32*
EM317	h$^-$ *rho1-596:nat, rad52-YFP:kan, ura4D18, leu1-32*
SM308[c]	h$^-$ *rad52-YFP:kan*, *leu1-32*, *ura4D18*
SM324	h$^-$ *rad52-YFP:kan*, *rgf1::his3$^+$, leu1-32*, *ura4D18*
EM250[f]	h$^-$ *leu1-32*, *ura4::RDUX200(kan+)*
EM303	h$^-$ *rgf1::nat*, *leu1-32*, *ura4::RDUX200(kan+)*
EM350	h$^-$ *rho1-596:nat, ura4::RDUX200(Kan+) leu1-32*
EM309	h$^-$ *lig4::kan*, *ura4D18, leu1-32*
EM372	h$^-$ *lig4::kan*, *rgf1::nat, ura4D18, leu1-32*
EM533[j]	h$^+$ *rad32::ura4+* (rad32 = mre11), ade6-M210 leu1-32 ura4-D18
EM591	h$^-$ *rad32::ura4$^+$* (*rad32 = mre11*), *rad52:YFP:kan, leu1-32*
EM144[b]	h$^+$ *rad51::kanMX6*, *ura4D18*, *leu1-32*
EM551	h$^-$ *rad51::nat*, *rad52:YFP:kan*, *ura4::RDUX200(kan+), leu1-32*
EM173	h$^+$ *rad51::kanMX6*, *rgf1::nat, ura4D18*, *leu1-32*
EM113[b]	h$^+$ *rad54::kanMX6*, *ura4D18*, *leu1-32*
EM120	h$^-$ *rad54::kanMX6*, *rgf1::nat, ura4D18*, *leu1-32*
EM561	h$^-$ *rad54::kanMX6*, *rad52:YFP:kan, ura4-D18*, *leu1-32*
EM117[g]	h$^-$ *rad54-GFP:hphMX6*
EM125	h$^-$ *rad54-GFP:hphMX6, rgf1::nat*
EM625[h]	h$^-$ *mus81::kanMX6, ura4-D18*, ade6-M210
EM635	h$^-$ *mus81::kanMX6, rad52:YFP:kan*
EM142[b]	h$^+$ *rad52::kanMX6*, *ura4D18*, *leu1-32*
EM170	h$^+$ *rad52::kanMX6*, *rgf1::nat, ura4D18*, *leu1-32*
EM111[i]	h$^+$ *rad9:YFP:ura4$^+$, rad52:CFP:kan, ura4D18*
EM650	h$^+$ *rad9:YFP:ura4$^+$*
EM652	h$^+$ *rad9:YFP:ura4$^+$*, *rgf1::nat*
EM631[h]	h$^-$ *rad11A-ts*, *ura4-D18*, *leu1-32*, *ade6-M216*
EM644	h$^-$ *rad11A-ts*, *rgf1::nat, ura4-D18*, *leu1-32*, *ade6-M216*
EM658	h$^-$ *rad11A-ts*, *rad52:YFP:kan, ura4-D18*, *leu1-32*
EM643[k]	h$^+$ *rad11-GFP:KanR*, *leu1-32, ade6M210, ura4D18*
EM644	h$^+$ *rad11-GFP:KanR*, *rgf1::nat, leu1-32, ade6M210, ura4D18*
EM34	h- *rgf1*Δ-45:*ura4$^+$*, *leu1-32*, *ura4-D18*, *his3-D1*, *ade6-M210*
EM44	h$^+$ *rgf1*Δ-45, *rgf2::kanMX6*, *ura4-D18*, *his3-D1*, *ade6-M210* (after FOA)
EM697	h$^-$ *rho1-596:nat, rad52-YFP:kan, rgf1::kanMX6, ura4D18, leu1-32*
EM699	h$^-$ *rho1-596:nat, rgf1::kanMX6, ura4D18, leu1-32*
EM718	h$^-$ *pck1*::*ura4$^+$rgf1*::*nat*, *leu1-32*, *ura4D18*
PG249	h$^+$ *pck2::kanMX6, rgf1*::*kanMX6*
PG335	h$^-$ *pmk1::ura4$^+$, rgf1*::*kanMX6, ura4d18*
EM701	h$^-$ *lig4::kan*, *rgf1::nat, rad51::kan, ura4D18, leu1-32*

All strains were generated in this study except for strains with label[a] obtained from P. Sunnerhagen (University of Gothenburg), label[b] from P. Perez (IBFG, University of Salamanca), label[c] from A. Bueno (CIC, University of Salamanca), label[d] from J.C. Ribas (IBFG, University of Salamanca), label[e] from J. Cansado (University of Murcia), label[f] from K. Komatsu (Radiation Biology Center, Kyoto University), label[g] from T. Nakagawa (Osaka University), label[h] from S. Forsburg (University of Southern California), label[i] from P. Meister and S. Gasser (FMI, University of Basel), label[j] from T. Nakamura (YGRC Japan), label[k] from T.C. Humphrey University of Oxford.

buffer (20 mM citrate/phosphate [pH 5.6], 40 mM EDTA, 1.2 M sorbitol) and then incubated for 90 min at 37°C in 5 ml of CSE containing 1.5 mg/ml Zymolyase-20T (Seikagaku Corporation, Japan) for cell wall digestion. The cell pellet was then resuspended in 300 μl of TSE buffer (10 mM Tris–HCl [pH 7.5], 0.9 M sorbitol, 45 mM EDTA) and mixed with 400 μl of 1% low melting point agarose in TSE and dispensed in 100 μl aliquots to plugs molds. Cell lysis was performed by incubating gelled plugs in 0.25 M EDTA, 50 mM Tris–HCl [pH 7.5], 1% SDS for 90 min at 55°C, followed by two 24 h incubations in 1% lauryl sarcosine, 0.5 M EDTA [pH 9.5], and 1 mg/ml proteinase K at 55°C. Plugs were stored at 4°C in Tris–EDTA and washed three times in Tris–EDTA before loading. Pulse-field gel electrophoresis was carried out in 0.8% chromosomal grade agarose (Bio-Rad) in a Bio-Rad CHEF-DRII apparatus. Electrophoresis (Pulse time: 1800 s, 2 V/cm, angle: 100°) was carried out for 48 h at 14°C in TAE buffer. Finally, the agarose gel was stained in 0.5 μg/ml ethidium bromide for 30 min.

Non-homologous DNA end joining (NHEJ)

We employed a NHEJ plasmid recircularization assay (43). Plasmid pFY20 was linearized using restriction endonucleases which generate 5′ over hangs (XmaI), 3′ over hangs (PstI) or blunt termini (SmaI); these linear plasmids are then transformed into cells and the transformation frequency was used to measure the efficiency of plasmid recircularization. The value for NHEJ efficiency was represented by an L/C ratio which was generated by dividing the transformation frequency obtained using linear plasmid DNA (L) with that obtained using covalently closed circular DNA (C) (uncut pFY20) and normalizes any strain to strain variance in the transformation efficiency.

Recombination assays

HR assays were performed as previously reported (44). A recombination reporter cassette *ura4::kanMX6* with a 200-bp tandem duplication (RDUX200(+)) was integrated into endogenous *ura4*$^+$ locus, which confers uracil prototrophy with the concomitant loss of G-418 resistance upon HR of the duplication. Cells were cultured in MMS medium containing 500 μg/ml of G418 overnight to eliminate the recombinants. The cells were collected by centrifugation, washed once with sterilized water and then resuspended in appropriate concentrations with sterilized water. Recombinants were detected with colony formation on uracil-free tester plates at a density of (2–5) × 10^5 cells per plate where *ura*$^+$ recombinants formed colonies. The mutation rate was determined by the Lea Coulson method of the median (45). Recombinant rates are the mean from at least three independent assays where three independent colonies were tested in each assay. The average recombinant rates and 95% CI were determined for these three means. Two-tailed unpaired Student´s test were used to determine the statistical significance of differences in recombination rates.

Microscopy and image analysis

Images and cell length measurements were obtained using an Olympus IX71 microscope equipped with a personal Delta Vision system and a Photometrics CoolSnap HQ2 monochrome camera, with Metamorph software (Universal Imaging, Molecular Devices, Downingtown, PA, USA). Measurements were made from micrographs using the IMAGEJ (National Institutes of Health). All microscopy was conducted on live midlog-phase cells placed on slides, except for cultures for DAPI and aniline blue staining, which were fixed in 70% ethanol at room temperature, washed, and pelleted before resuspension in 5 μl of DAPI solution (500 μg/ml). More than 200 dividing cells per strain were measured for the cell length data. Stacks of ten z-series sections were acquired at 0.2-μm intervals. All fluorescence images are maximum two-dimensional (2D) projections of z-series and were analyzed using deconvolution software from Applied Precision. To calculate the area of the nucleus occupied by Rad52p-YFP a binary mask was created using the mean value of the nuclear background without foci as a threshold and measuring the area of this mask. To detect Rad51p indirect immunofluorescence microscopy was performed according to the protocol described in (46). The rabbit polyclonal anti-human Rad51p (PA5-27195, Thermo Fisher, Rockford, IL, USA) was diluted 1.100.

RESULTS

Rgf1p promotes viability in cells treated with phleomycin

We have previously reported that *rgf1*Δ cells were significantly delayed in the recovery from replication arrest caused by hydroxyurea (HU) treatment. Upon the removal of HU, the septation peak occurred after 2 h in the wild-type, whereas in the mutant it was delayed up to 4 h (41). To understand the role of Rgf1p in recovery from genotoxic damage, we tested the sensitivity of *rgf1*Δ to additional DNA-damaging agents such as ultraviolet light (UV), methyl-methane sulfonate (MMS), camptothecin (CPT) and the drug phleomycin (Phl). UV irradiation and MMS halt DNA replication by producing cyclobutane pyrimidine dimers and fork DNA alkylation, respectively. CPT is a topoisomerase I inhibitor that breaks DNA replication forks (47), and Phl (a derivative of Bleomycin) induces single-strand and double-strand breaks (DSBs) and other types of oxidative damage (48,49). All of these agents induce damage, however, while MMS, UV and CPT are known to interfere with S phase progression (50,51), the DSBs that result from treatment with Phl are believed to be repaired at the G2 phase of the cell cycle. The *rgf1*Δ mutant cells were as resistant as wild-type cells to high doses of MMS and UV (Figure 1). In contrast, deletion of Rgf1p produced cells that were sensitive to CPT and highly sensitive to chronic exposure to Phl (Figure 1). Ionizing radiation (IR) slightly decreased survival of *rgf1*Δ cells compared to wild-type cells (Supplementary Figure S1). These results suggest that Rgf1p is specifically required for tolerance to genotoxins that produce double-strand breaks.

Recovery from a DNA-damage-induced G2 arrest requires Rgf1p

We examined viability in *rgf1*Δ and wild-type cells in the presence of acute Phl treatment. Similar to checkpoint mutants, *rgf1*Δ cells lost viability in the presence of Phl (Fig-

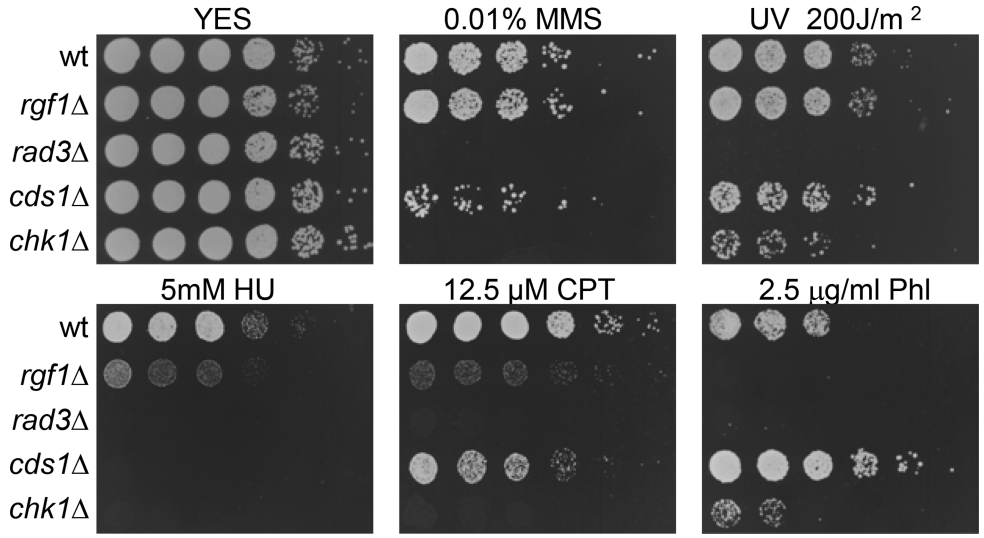

Figure 1. *rgf1*Δ cells are highly sensitive to Phl. Serial dilutions (1, 0.5, 0.25, 0.025, 0.0025 and 0.00025) of the indicated strains were spotted onto rich YES plates containing the indicated DNA-damaging agents or irradiated by UV. Colony formation was analyzed after 3 days at 28°C.

ure 2A). However, examination of the cells by microscopy indicated that *rgf1*Δ cells had an arrested nuclear cycle that allowed repair to occur, but continued to grow. This observation indicated that the cells had initiated a DNA damage-dependent checkpoint properly (Figure 2B). This conclusion was confirmed by immunoblot analysis of the DNA damage checkpoint kinase Chk1p (Figure 2C), which is hyper-phosphorylated when activated. We also noticed that treatment of *rgf1*Δ cells with Phl for 6h resulted in the formation of very elongated cells (Figure 2B), which suggests a failure to downregulate growth. This might be relevant because in budding yeast checkpoint proteins are known to be involved in the restriction of polarized cell growth in response to DNA replication stress (52,53).

Following on, growth, nuclear morphology, cell length and DNA content after terminating the Phl treatment was measured. In the *rgf1*Δ cells, the damage elicited by the treatment was not reversed, and the cells were unable to duplicate during the duration of the experiment. In contrast, wild-type cells re-entered the cell cycle and started to divide normally (Figure 2D and E). The *rgf1*Δ strain harbored a large number of abnormally long cells (Supplementary Figure S2), some of them showing an elongated nucleus (Figure 2D). Progression into S phase after Phl treatment seemed to be similar in both strains (see the 4C peak 2 h after Phl). However, after 6–8 h, wild-type cells displayed a marked increase in the number of cells with a 2C DNA content, while *rgf1*Δ cells ended up with a flat 2C and 4C population that never exited mitosis (Figure 2F). Accordingly, upon removal of Phl, dephosphorylation of Chk1p was delayed in *rgf1*Δ cells (Figure 2G). This delay in dephosphorylating Chk1p, together with the phenotypes seen during recovery, indicated that Rgf1p mutant cells were defective in reentry into the cell cycle following the induction of severe DNA damage.

The Rgf1p/Rho1p signaling pathway is involved in recovery from DNA-damage induced G2 arrest

Rgf1p acts as a guanine nucleotide exchange factor for Rho1p, but not for other Rho-family GTPases (32,34). Previous work carried out in *S. cerevisiae* and *S. pombe* indicates that Rho1p is necessary during contractile actomyosin ring (CAR) assembly and septum formation in the last steps of cytokinesis (30,54,55). However, there is no evidence of it playing a role in mitotic progression after DNA damage in either yeast. To address this question, we checked whether the catalytic activity of Rgf1p was required for efficient recovery after checkpoint arrest. We found that a deletion mutation in the RhoGEF domain of Rgf1p (*rgf1-PTTR*Δ), which results in significantly reduced GEF activity towards Rho1p (37), phenocopied the sensitivity of the Rgf1p deletion mutant to Phl (Figure 3A). Rgf1p contains several domains that are important for proper functioning: a pleckstrin-homology (PH) essential for activity; a regulatory N-terminus followed by a *Dishevelled*, *Egl-10*, and *Pleckstrin* (DEP) domain, involved in nucleus-cytoplasmic shuttling, and a Citron and NIK1-like kinase homology-domain (CNH) of unknown function (41). Here, we show that besides the Rho-GEF domain, cells containing a deletion in the PH domain (Rgf1pΔPH) also lost viability after Phl treatment (Figure 3A), suggesting that the ability to reenter the cell cycle after DNA damage relies on Rgf1p catalytic activity, probably towards Rho1p.

Supporting these data, a hypomorphic and thermosensitive mutant of Rho1p, *rho1-596,* elicited the same effects as the Rgf1p deletion (40). Similar to the *rgf1*Δ mutant cells, the *rho1-596* mutant was sensitive to HU (Supplementary Figure S3), CPT and Phl (Supplementary Figure 3B). *rho1-596* cells arrested the nuclear cycle that allows repair to occur (not shown). However, unlike wild-type cells, after Phl treatment the mutant cells remained elongated and did not reenter the cell cycle (Figure 3C). Sensitivity to Phl and CPT was not exclusive to the *rho1-596* mutant, since cells lacking the Rho1p-upstream regulator (Rgf3p) and the Rho1p-

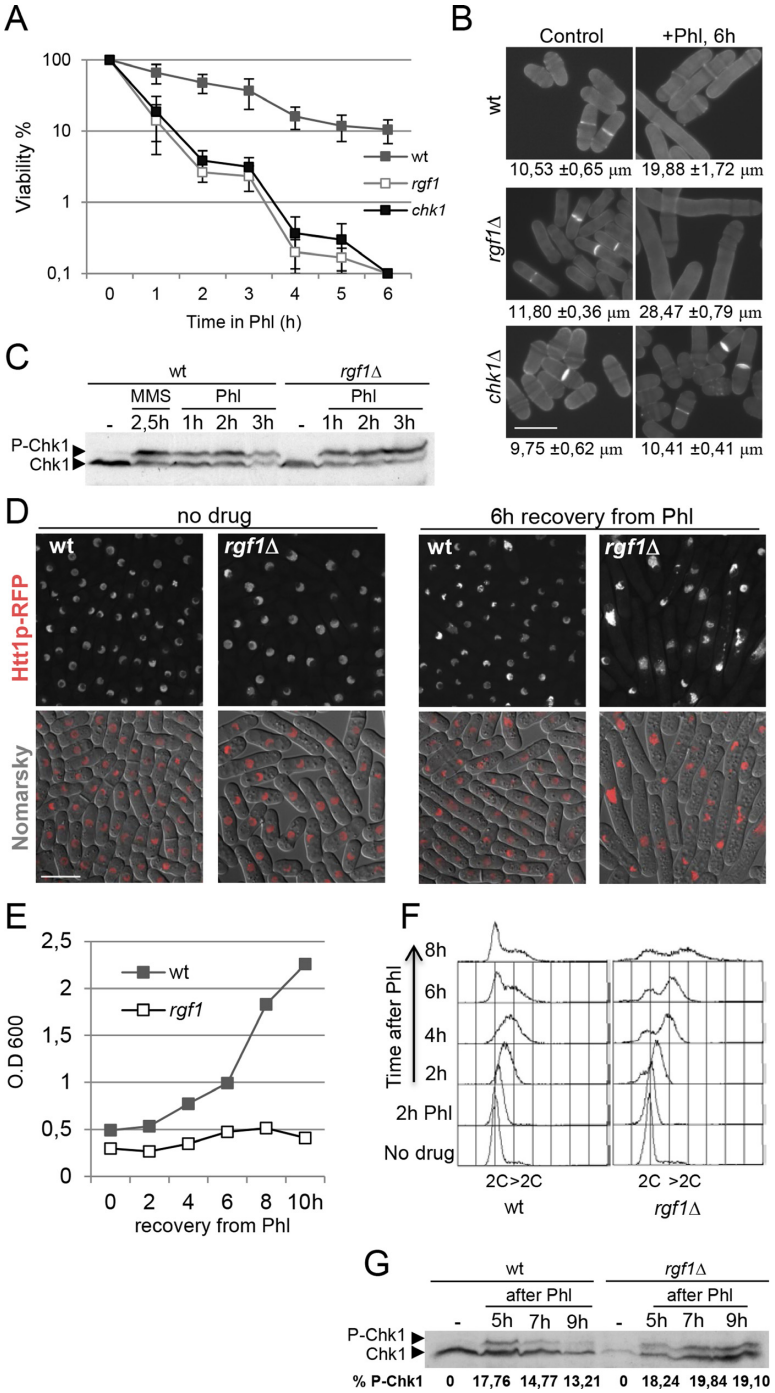

Figure 2. Rgf1p is required for deactivation of the DNA damage checkpoint but not for its activation. (**A**) Rgf1p is required to maintain cellular viability in response to short exposures to Phl. Cells were grown to logphase and shifted to 10µg/ml of Phl for 6 h. Samples were taken every hour to determine cell viability by assessing plating efficiency on rich medium w/o Phl. Survival was estimated relative to untreated cells. The data plotted here are averaged from three independent experiments and error bars represent S.D. around the mean. (**B**) Samples of the indicated strains, before and after a 6 h exposure to the drug, were stained with aniline blue to visualize cell length and septa. Bar 10 µm. The average length of cells within the cell population in three independent experiments are shown (mean ± S.D.; $n > 50$ for each value). (**C**) Wild-type or *rgf1*Δ cells containing an HA-tagged Chk1p were grown to logphase and treated with 10 µg/ml Phl. Protein extracts from each of the indicated time-points were analyzed by western blot and the membranes were probed with anti-HA to visualize Chk1p. Chk1p activation was also analyzed in wild-type cells treated with 0.03% MMS. (**D**) *rgf1*Δ cells do not recover from the cell-cycle block caused by Phl. Wild-type and *rgf1*Δ cells growing exponentially at 28°C in YES medium were treated with Phl for 10 min, released into fresh medium without Phl, and then grown for another 6 h at 28°C. Cells were examined by interferential contrast (DIC) and Htt1-RFP (histone H3 h3.1) fluorescence. Bar 10 µm. (**E**) Growth curve of wild-type and *rgf1*Δ cells treated with Phl for 2 h, released into fresh medium without Phl, and then grown for another 10 h at 28°C. (**F**) FACS analysis of wild-type and *rgf1*Δ cells. Samples were taken before and after Phl treatment at 2 h intervals and processed to analyze the DNA content by flow cytometry. (**G**) Cells were arrested for 10 min in 10 µg/ml Phl, washed thoroughly, and resuspended in fresh medium. Protein samples were analyzed by western blot as described above. The numbers represent the percentages of Chk1p phosphorylation relative to Chk1 protein. The intensity of the signal was quantified using ImageJ.

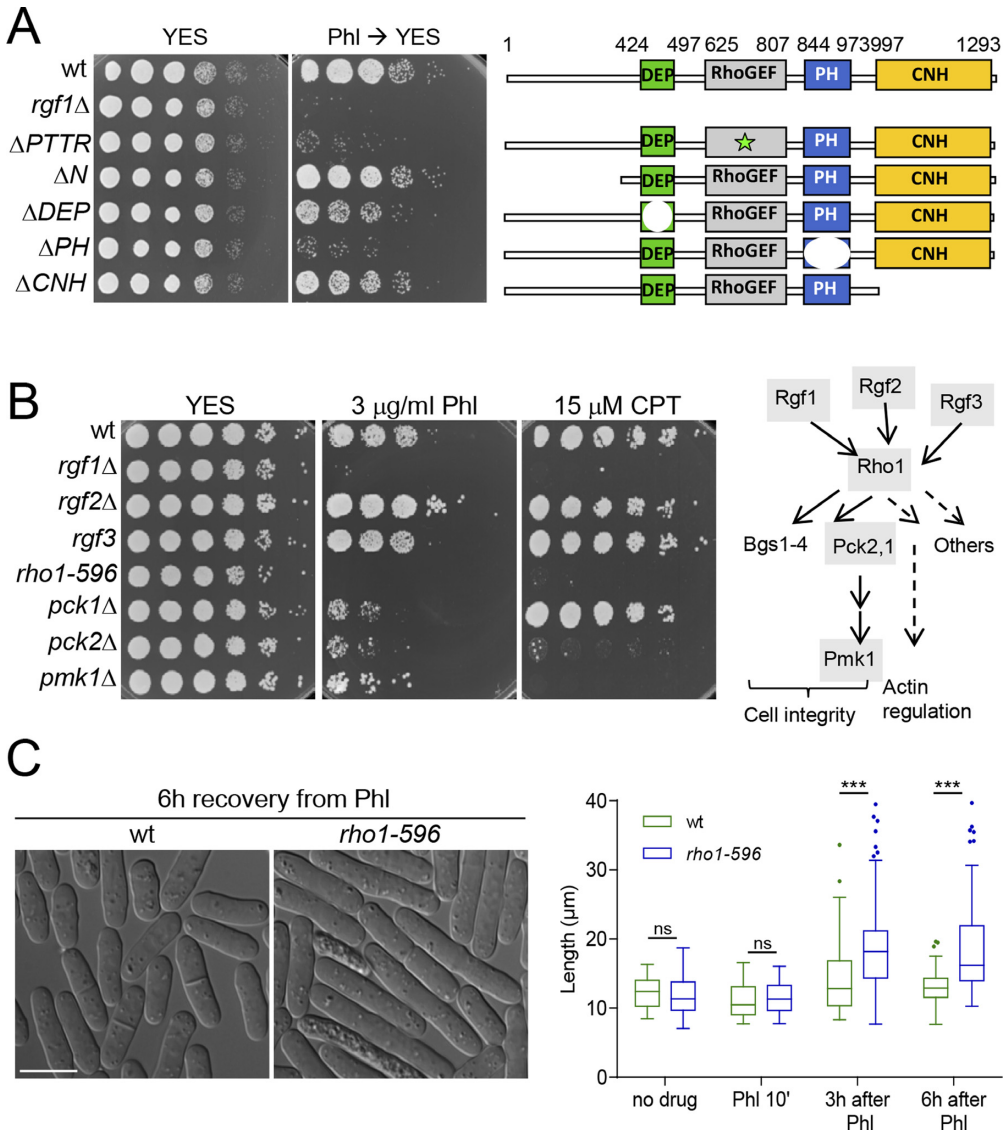

Figure 3. Rho1p is involved in recovery from DNA-damage induced G2 arrest. (**A**) The Rho-GEF and PH domains are essential for Rgf1p function *in vivo*. For Phl hypersensitivity, serial dilutions (1, 0.5, 0.25, 0.025, 0.0025 and 0.00025) of the wild-type, *rgf1*Δ, Rgf1pΔPTTR, Rgf1pΔN, Rgf1pΔDEP, Rgf1pΔPH and Rgf1pΔCNH cells previously treated with 10 μg/ml Phl for 4 h were plated and incubated at 28°C on YES plates w/o drug. Schematic representation of the domain structure of the full-length Rgf1p (aa 1–1334) and the various deletion mutations used. (**B**) The Rho1p signaling pathway was necessary for survival in the presence of Phl and CPT. Left, serial dilutions of the indicated strains prepared as in A were spotted onto rich YES plates containing the indicated DNA-damaging agents. Colony formation was analyzed after 3 days at 28°C for Phl- and 32°C for CPT-included assays. Right, a scheme of the Rho1p cell-signaling pathway is shown (36). The gray shading indicates the proteins whose mutants were analyzed in B. (**C**) Wild-type and *rho1-596* mutant cells were cultured to mid-log phase in YES medium at 28°C, treated with Phl for 10 min and then released into fresh medium without Phl at the same temperature. Cells were photographed 6 h after release (left). Bar 10 μm. Tukey boxplot illustrating quantitative analysis of the size distribution of individual cells ($n > 100$) in a population of each strain and condition (right). One experiment representative of 3 is shown. Statistical significance was calculated using two-tailed unpaired Student's *t* test. ***$P < 0.001$; ns = non-significant.

downstream effectors (Pck1p, Pck2p and Pmk1p) were unable to grow in the presence of the genotoxic agents that affected the *rgf1*Δ strain (Figure 3B and scheme of Rho1p signaling pathway). Deletion of $rgf3^+$ is lethal thus we used the *ehs2-1* mutant (*rgf3*) to test sensitivity to genotoxic drugs using drop assays at 37°C (35). *pck2*Δ and *pmk1*Δ cells were sensitive to HU (Supplementary Figure S3), CPT and Phl (Figure 3B) and *pck1*Δ and *rgf3* mutant cells were hypersensitive to Phl and HU (Figure 3B and Supplementary Figure S3). We were unable to test sensitivity to CPT of the *rgf3* cells because CPT inhibited growth of all strains at 37°C (Supplementary Figure S3). The *rgf2*Δ cells grew like wild-type cells under the conditions tested (Figure 3B). However, when Rgf1p activity is compromised, *rgf2*Δ cells become sensitive to Phl and HU at 32°C. This was shown by the fact that *rgf1-45*Δ cells (that lack the last 45 aa of Rgf1p) were able to grow on Phl and HU plates at 32°C, while the *rgf1-45*Δ*rgf2*Δ mutant was inviable in the same conditions (Supplementary Figure S3). Finally, an *rgf1*Δ *rho1-596//pck2*Δ/*pmk1*Δ double mutant exhibited no synergis-

tic increase in Phl sensitivity (Supplementary Figure S3). These results indicate that Rho1p and some of the proteins involved in Rho1p signaling function in the recovery from a DNA-damage G2 induced arrest.

Checkpoint removal does not rescue sensitivity to Phl in *rgf1*Δ cells

In *S. pombe* Chk1p and Cds1p kinases respond to different checkpoint signals. Chk1p is required for the DNA damage checkpoint and Cds1p is specifically involved in the replication checkpoint (56). However, their roles seem to be shuffled in metazoans; for instance, hChk2p (Cds1p homologue in mammals) functions to arrest the cell cycle after DSBs. Here, it was observed that: (i) Chk1p, but not Cds1p, was phosphorylated in the presence of Phl (Supplementary Figure S4); (ii) Chk1p, but not Cds1p, was required for survival when DNA was damaged by Phl (Figure 1) and (iii) deletion of Rgf1p impaired Chk1p dephosphorylation after DNA damage (Figure 2G).

Thus, we asked whether the elongated phenotype seen in *rgf1*Δ cells during recovery from Phl treatment was dependent on their inability to turn off the G2 DNA damage checkpoint. We deleted the checkpoint kinase Chk1p in an *rgf1*Δ background. The *rgf1*Δ cells were slightly longer than the wild-type cells (the size at division was 16.09 ± 1.4 μm and 14.71 ± 0.9 μm, respectively). In an unperturbed cell cycle, elimination of Chk1p had little influence in cell length and viability of the *rgf1*Δ mutant (Figure 4A). In the recovery from DNA damage (3 h) the double knockout *rgf1*Δ*chk1*Δ cells behaved like *chk1*Δ, suggesting that abrogation of the checkpoint by Chk1p permitted *rgf1*Δ cells to proceed into mitosis (Figure 4A and B). If arrest in the *rgf1*Δ mutant resulted exclusively from cell cycle checkpoint activation due to persistent signaling, we might expect that checkpoint elimination could rescue sensitivity to Phl in *rgf1*Δ cells. However, the double knockout *rgf1*Δ*chk1*Δ cells were just as sensitive to Phl as the single-knockout *rgf1*Δ cells and more sensitive than the *chk1*Δ mutant (Figure 4C). Altogether, these results suggest that the role of Rgf1p in checkpoint termination could reflect the inability of *rgf1*Δ cells to re-enter the cell cycle in the presence of unrepaired DNA lesions.

Rgf1p is required to efficiently repair fragmented chromosomes generated by Phl treatment

Next, we asked whether the phenotypes seen in the *rgf1*Δ during recovery from Phl treatment were due to the presence of unrepaired DNA. To this end the integrity of the yeast genome of wild-type, *rgf1*Δ and *rad51*Δ strains was monitored by PFGE (Pulse Field Gel Electrophoresis) analysis before and at various times after Phl treatment. We found that an incubation of fission yeast cells with 10 μg/ml of Phl caused fragmentation of chromosomes, demonstrating the induction of DSBs (Figure 5A and Supplementary Figure S5A). In the wild-type, this pattern was restored when examined 15 h after treatment, indicating the completion of DSB repair. In contrast, fragmented chromosomes were repaired inefficiently in *rgf1*Δ cells and left unrepaired in *rad51*Δ cells (Figure 5A and Supplementary Figure S5A). Thus, the persistence of chromosome fragmentation in the *rgf1*Δ mutant suggests that *rgf1*Δ cells were defective in repairing DSB.

Deletion of *rgf1*$^+$ accumulates Phl-induced Rad52p-YFP foci

Next, we tested the number of DSBs arising from the treatment with Phl in wild-type and *rgf1*Δ cells. We scored for the appearance of Rad52p-YFP foci by fluorescence microscopy. Rad52p forms a multimeric complex at broken DNA ends and at internal DNA loops (57). The complex can be visualized as a focus under a microscope and the focus is thought to represent a site of HR (19,20). It is difficult to distinguish between sites of DNA breaks arising from erroneous replication (replication foci) from foci generated after DNA damage (repair foci). Hence, we scored for cells with two or more foci per nucleus, which is more likely to represent repair foci. Remarkably, in the absence of Phl, the number of multiple Rad52p-foci positive cells ($n \geq 2$) in the *rgf1*Δ mutant was 3-fold higher than that of the control cells (∼2% in the wt versus ∼7% in *rgf1*Δ mutant) (Figure 5B). Following 2 h exposure to Phl, >70% of the cells in the wild type and in the *rgf1*Δ mutant had multiple Rad52p-YFP foci (Figure 5B). Similar increases were seen in both strains after incubation with Phl for 1.5 h, 1 h, 30 min and 10 min (Supplementary Figure S5B), indicating that the number of cells with ≥2 foci was not a direct function of time. Thus, for the rest of the experiments we used 10 min Phl treatments to induce DSBs. These observations imply that multiple DSBs are processed in the same recombination 'factory' which disappears only when DNA repair is completed (19). Next, we examined the dissolution rate of Phl-induced Rad52p-YFP foci in the recovery from drug treatment. In wild type, the percentage of nuclei displaying 2 or more Rad52p-YFP foci decreased to an average of 35% after 4 h. In contrast, >80% of the *rgf1*Δ mutant nuclei still contained multiple foci (Figure 5B). These results indicate that the absence of Rgf1p strongly inhibits repair generating long lasting Rad52p-YFP foci.

It is known that proteasome functioning regulates Rad52p and subsequent HR (58). Thus, it was ensured that the long lasting Rad52p-YFP foci did not arise from a defect in Rad52p degradation. Western blot analysis of extracts from cells treated with cycloheximide (CHX) after Phl treatment revealed that the amount of Rad52p-YFP was similar in wild-type and in *rgf1*$^+$-deleted cells in the recovery from Phl (Supplementary Figure S6). Importantly, Rad52p-YFP cells exhibited the same sensitivity to Phl compared with wild-type cells (unpublished data).

Next, the extent of the damage in wild-type and *rgf1*Δ cells was determined. Following Phl, the area of the nucleus occupied by Rad52p-YFP foci in $n = 50$ cells of each strain was similar; however, 3 h after recovering in Phl-free medium, foci were spread over an area 3 times bigger in the *rgf1*Δ cells than in wild-type cells (Figure 5C). Moreover, the mean number of Rad52p-YFP foci per focus-positive nucleus in the *rgf1*Δ increased to 6 at t = 3h compared to the initial starting point right after initiating Phl treatment (Figure 5C, compared *rgf1*Δ in Phl and 3 h after Phl). Finally, we tested whether the *rho1-596* cells (Figure 3B and Supplementary Figure S3) also contained the same defect

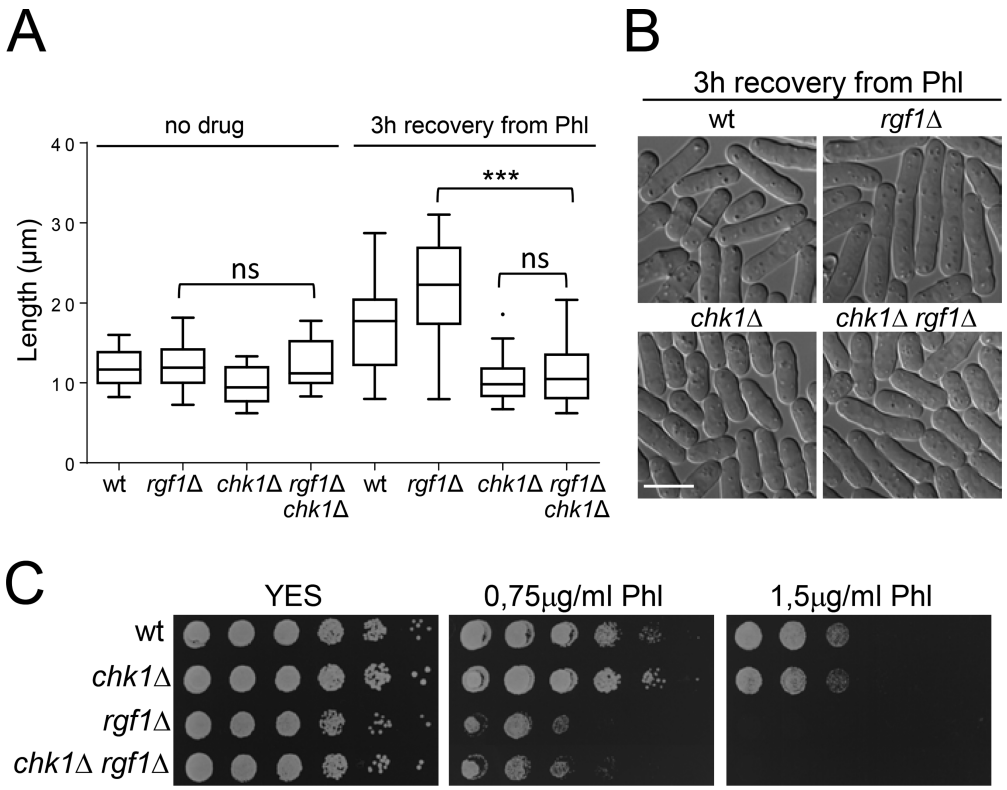

Figure 4. Checkpoint removal does not rescue sensitivity to Phl in *rgf1*Δ cells. (**A**) The strains indicated were cultured to midlog phase in YES medium at 28°C, treated with Phl for 10 min, and then released into fresh medium without Phl for 3 h at 28°C. Tukey boxplot illustrating quantitative analysis of the size distribution of individual cells ($n > 100$) in a population of each strain and condition (left). One experiment representative of three is shown. Statistical significance was calculated using two-tailed unpaired Student's *t* test. ***$P < 0.001$; ns = non-significant. (**B**) Logphase cells of the strains indicated grown as in (A) were examined by DIC 3h after release from Phl treatment. Bar 10 µm. (**C**) Serial dilutions (1, 0.5, 0.25, 0.025, 0.0025 and 0.00025) of the indicated strains were spotted onto rich YES plates with or w/o Phl. Colony formation was analyzed after 3 days at 28°C.

as the *rgf1*$^+$ deletion mutant. The dissolution rate of Phl-induced Rad52p-YFP foci in *rho1-596* and *rgf1*Δ *rho1-596* cells at 28°C (permissive temperature) was very similar to that of the *rgf1*Δ cells (Figure 5D), suggesting that Rho1p functions in DSB repair.

Lack of Rgf1p decreases spontaneous HR activity

Two major pathways repair DSBs: non-homologous end joining (NHEJ), and homologous recombination (HR) (22). Sensitivity to IR (Phl) is characteristic of HR mutants and only seen in NHEJ mutants when arrested in G1 (59). Thus, one possibility to explain the persistence of Rad52p-YFP foci in *rgf1*Δ cells is that HR is less operative in cells lacking the Rgf1p GEF. We performed a reporter recombination cassette *RDUX200(+)* assay to establish whether Rgf1p was required for HR (44,58). The reporter *ura4::KanMX6 (RDUX200)* has a duplication of the central portion of the *ura4*$^+$ gene, bracketing the neomycin-resistance module *kanMX6*. Upon HR of the duplication, the *RDUX200* conferred uracil prototrophy with the concomitant loss of G-418 resistance (Figure 6A). The analysis revealed that lack of *rgf1*$^+$ decreased the rate of spontaneous HR approximately 4 fold compared with control wild-type cells. Similarly, *rho1-596* cells showed a reduction in the rate of spontaneous HR, while *rad51*Δ cells behaved as a hyper-recombinant (Figure 6A). In fission yeast, two Rad52p-dependent pathways are responsible for the majority of recombination between repeated DNA sequences. One of these pathways involves the Rad51p epistasis group of proteins, and is required for generating conversion-type recombinants, whilst the other is independent of Rad51p and only generates deletion-type recombinants (60). These results suggest that Rgf1p and Rho1p might play a role in repair in a pathway that generates deletion types.

HR and NHEJ collaborate and compete with each other at double-strand break sites to enhance DNA repair (16). Therefore, we tested proficiency of the *rgf1*Δ cells to carry out NHEJ. The NHEJ assay involves transformation of cells with a replication origin-containing plasmid (43). The plasmid (pFY20) was linearized within sequences that lack homology to genomic sequences to generate 5′, 3′ or blunt termini. The linear plasmids were then transformed into wild-type, *rgf1*Δ and *lig4*Δ cells, and the transformation frequency was used to measure the efficiency of plasmid circularization proceeding through NHEJ. An uncut plasmid (uncut pFY20) was transformed in parallel to normalize the transformation efficiencies. As expected, plasmid end-joining efficiency in *rgf1*Δ cells was comparable to wild-type, but different to that of *lig4*Δ cells, which are NHEJ deficient irrespective of the structure of the linear DNA termini (Figure 6B, (61)). We conclude that Rgf1p is not required for NHEJ.

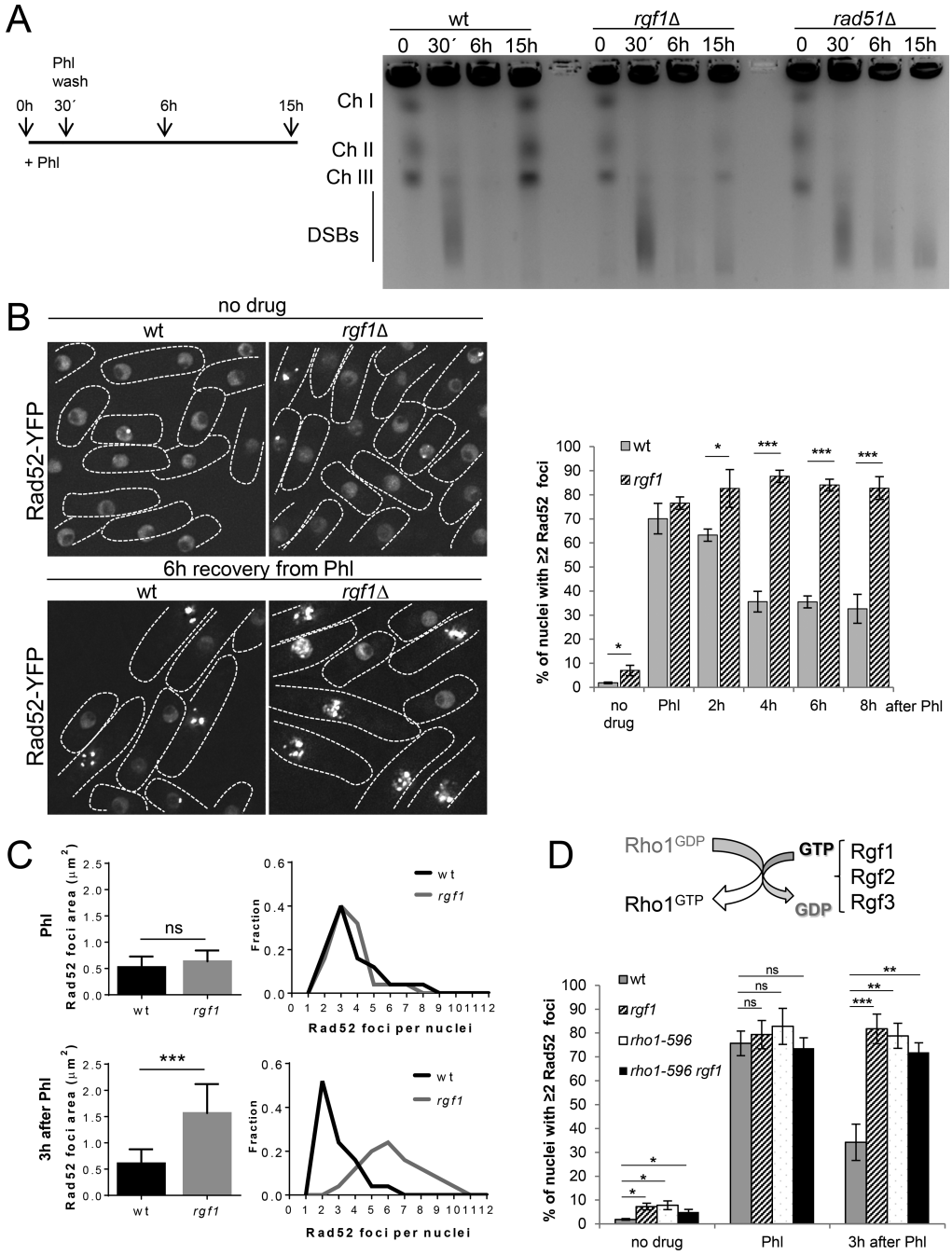

Figure 5. Rgf1p is required for the repair of Phl-induced Rad52p-YFP foci. (**A**) PFGE analysis of the Phl-treated cells. Wild-type, *rgf1*Δ and *rad51*Δ cells were treated with 10 μg/ml Phl for 30 min, and agarose plugs were prepared before treatment, immediately, at 6 h (2.0 generations) and at 15 h (3.5 generations) after treatment, as indicated in the scheme. The three chromosomes were fragmented by Phl treatment in the three strains, but re-assembled within 3.5 generations, only in the wild-type cells. (**B**) Live imaging of Rad52p-YFP in wild-type and *rgf1*Δ cells in the absence of Phl (top) and 6 h after release from Phl-induced arrest (bottom). Note that *rgf1*Δ cells have a larger number of Rad52p-YFP factories than wild-type cells. Quantitation of the fraction of nuclei containing ≥2 Rad52p-YFP foci in wild-type and *rgf1*Δ mutant cells without Phl and during the recovery from Phl treatment. Cells from the indicated strains were cultured to mid-log phase in YES medium, treated with Phl for 2 h and then released into fresh medium without Phl for 8 h. The number of foci in at least 200 nuclei for each strain and condition were scored in three independent experiments. Mean values were plotted with error bars representing the S.D. around the mean. Statistical significance was calculated using two-tailed unpaired Student's *t* test. The *asterisk in*dicates that the *rgf1*Δ value is significantly different from that of the wild type. $*P < 0.05$, $***P < 0.001$. (**C**) The area occupied by Rad52p-YFP in wild-type and *rgf1*Δ cells with ≥2 foci immediately after Phl treatment (top) and 3 h after treatment (bottom). The nuclear area is expressed as a function of the total nuclear volume assuming a radius for a typical haploid nucleus of 2.5 μm. Values represent the mean ± S.D. of three experiments; $n > 50$ for each value. Statistical significance was calculated using two-tailed unpaired Student's *t* test. $***P < 0.001$; ns = non-significant. The number of Rad52p-YFP foci was quantified for each strain and condition on the right. (**D**) Scheme of Rho1p GEFs function. Quantitation of the fraction of nuclei containing ≥2 Rad52p-YFP foci in wild-type, *rgf1*Δ, *rho1-596* and *rho1-596 rgf1*Δ cells. Mid-log cells were treated with Phl for 10 min and then released into fresh medium without Phl for 3 h at 28°C. The number of foci was scored and represented as in B. The *asterisk* indicates that the *rho1-596* and *rho1-596rgf1*Δ values are significantly different from that of the wild type. $*P < 0.05$, $**P < 0.01$. ns = non-significant.

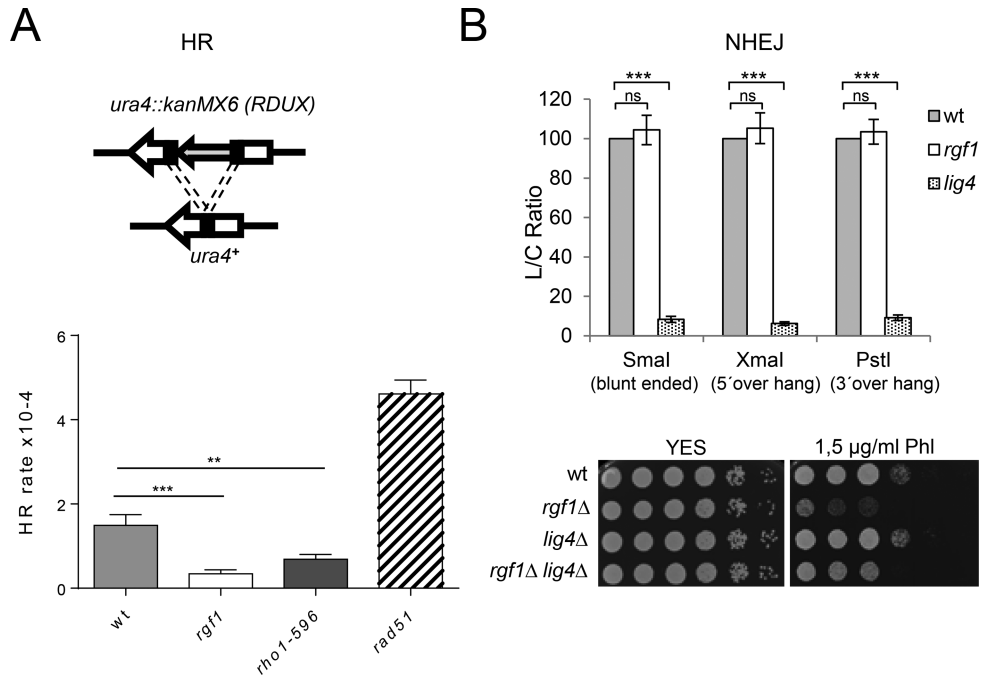

Figure 6. Lack of Rgf1p decreases spontaneous HR activity. (**A**) An example of a recombination reporter gene *ura4::kanMX6* (*RDUX*) with a 200-bp tandem duplication (*RDUX200*(+)) and its reversion product (*ura4*+). (lower panel) Spontaneous recombination rate in wild-type, *rgf1*Δ, *rho1-596* and *rad51*Δ cells was measured by using the *RDUX200* reporter as described in the Materials and Methods. The experiments were performed three times and error bars represent 95% CI. Statistical significance was calculated using two-tailed unpaired Student's *t* test. The *asterisk* indicates that the *rgf1*Δ and *rho1-596* value are significantly different from that of the wild type. $^{**}P < 0.01$ and $^{***}P < 0.001$. (**B**) A value for NHEJ efficiency is represented by an L/C ratio which was generated by dividing the transformation frequency obtained with linear plasmid DNA (L) with that obtained with covalently closed circular DNA (C) (uncut pFY20), which normalized any strain to strain variance in the transformation efficiency (rather than NHEJ efficiency). Values are the means from three independent experiments, and S.D. *Bars* are indicated. Statistical significance was calculated using two-tailed unpaired Student's *t* test; ns = non-significant. $^{***}P < 0.001$. (Lower panel) Serial dilutions (1, 0.5, 0.25, 0.025, 0.0025 and 0.00025) of the indicated strains were spotted onto rich YES plates with or w/o Phl. Colony formation was analyzed after 3 days at 28°C.

If the Rgf1p defective cells were sensitive to Phl because they were unable to carry out DSB repair by HR, the elimination of NHEJ in *rgf1*Δ mutants might be expected to further impair Phl survival; however, in fact the opposite was true. A *rgf1*Δ *lig4*Δ strain is slightly more resistant to Phl than an *rgf1*Δ strain (Figure 6B). Mutants in NHEJ factors, such as Ku and the yeast homolog of DNA ligase IV, showed an enhanced rate of end resection and increased HR compared to wild-type cells (62,63), which could explain the partial suppression the *rgf1*Δ repair defect.

Deletion of *rgf1*$^{+}$ accumulates Phl-induced Rad11p-GFP, Rad54p-GFP and Rad51p foci

To determine which step in the repair of DSBs could cause the stabilization of Rad52p foci in *rgf1*Δ cells, we compared the dynamics of Rad52p-YFP foci seen in *rgf1*Δ with that of known HR and checkpoint mutants (Figure 7A). The list of factors involved in repair by HR were divided into four categories: (a1) Rad32p/Mre11p and Ctp1p consisting of nucleases and helicases, that generate 3´ single-stranded DNA (ssDNA) overhangs; (a2) the core repair proteins Rad11p (large subunit of replication protein A, RPA), Rad51p, Rad54p and Rad52p, where Rad52p catalyzes the assembly of Rad51p recombinase as a nucleoprotein filament and this structure can invade homologous duplex DNA, which is used as a template for DNA synthesis; (a3) regulators of HR execution such as Mus81p and Rqh1p; and (a4) checkpoint proteins, Rad3p, Crb2p and Chk1p.

Rad52p foci formation after Phl was independent of the core repair proteins (Figure 7A). However, checkpoint mutants and cells deleted for *mre11*$^{+}$ showed a reduction in focal assembly of Rad52p; the latest is consistent with a role of Mre11p in the MRN complex (Mre11p, Rad50p and Nbs1p) involved in resection (Figure 7A). In cells deleted for the resolvase Mus81p, 30% of the nuclei contained multiple foci before treatment, where this number became duplicated after Phl treatment (Figure 7A).

During post Phl treatment, the percentage of wild-type cells with multiple Rad52p foci declined steadily during the G2/M arrest period and dispersed as the cells reentered the cell cycle (Figure 7A). *Mre11* mutant cells never solved the foci and in the checkpoint mutants (*rad3*Δ, *crb2*Δ and *chk1*Δ) the foci disappeared but less efficiently than in wild-type cells (Figure 7A). Cells deleted for *rgf1*$^{+}$ behaved like *rad11*, *rad51*Δ, *rad54*Δ and *mus81*Δ mutants, and in all of them the number of cells with multiple Rad52p foci did not decline noticeably during recovery (Figure 7A). Moreover, combination of *rgf1*Δ with mutants in the core repair proteins – *rad11*, *rad51*Δ, *rad52*Δ and *rad54*Δ- produced mutant cells more sensitive to Phl than any of the single mutants (Supplementary Figure S7). These results suggest

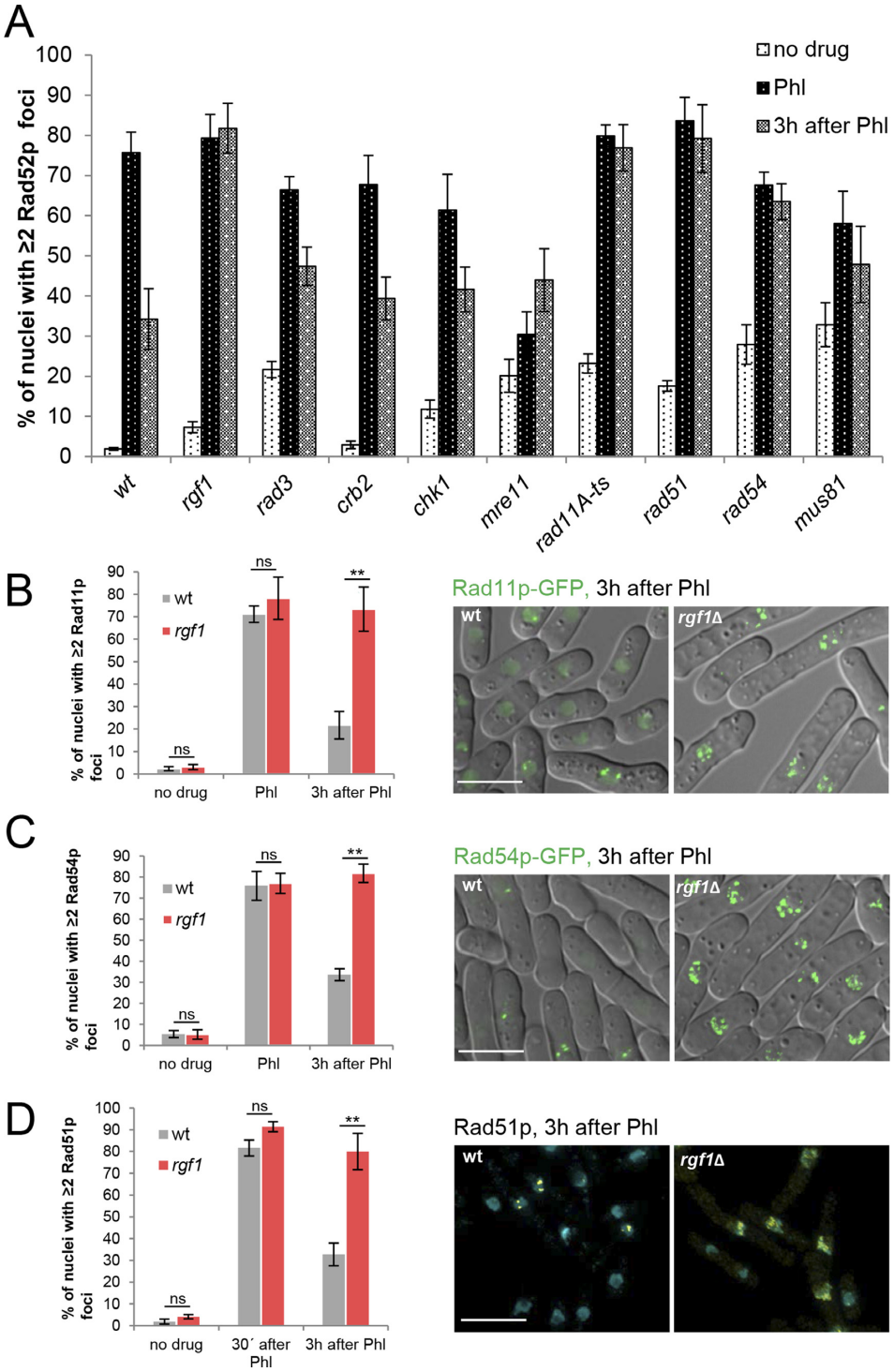

Figure 7. Deletion of *rgf1*$^{+}$ accumulates Phl-induced Rad11p, Rad54p and Rad51p foci. (**A**) Quantitation of the fraction of nuclei containing Rad52p-YFP foci in wild-type, *rgf1*Δ and mutants in the HR process. Cells from the indicated strains were culture to mid-log phase in YES medium, treated with Phl for 10 min and then released into fresh medium without Phl for 3 h. The number of foci in at least 100 nuclei for each strain and condition were scored in three independent experiments. Mean values were plotted with *error bars* representing the S.D. around the mean. (**B**) Quantitation of the fraction of nuclei containing Rad11p-GFP foci in wild-type and *rgf1*Δ cells before, in Phl and 3 h after treatment. The number of foci in at least 100 nuclei for each strain and condition were scored in three independent experiments. Error bars represent the standard deviation of the mean. Statistical significance was calculated using two-tailed unpaired Student's *t* test. $^{**}P < 0.01$; ns = non-significant. (right) Representative live imaging of Rad11p-GFP in wild-type and *rgf1*Δ cells 3 h after release from Phl arrest. (**C**) Quantitation of the fraction of nuclei containing Rad54p-GFP foci in wild-type and *rgf1*Δ cells. Culturing and quantitation was performed as in B. (right) Representative live imaging of Rad54p-GFP foci. (**D**) Quantitation of the fraction of nuclei containing ≥2 Rad51p foci in wild-type and *rgf1*Δ cells. Treatment of the cells was the same as that performed in B. The nuclei were stained with anti-Rad51p (yellow) and DAPI (blue) and the number of Rad51p foci were scored before, 30 min and 3 h after Phl. Statistical significance was calculated using two-tailed unpaired Student's *t* test. $^{**}P < 0.01$. (Right) Examples of Rad51p foci from wild-type and *rgf1*Δ cells 3h after release from Phl. Bar 10 μm.

that core repair HR proteins and Rgf1p operate in separate pathways to confer Phl resistance.

Next, the protein composition of DNA repair foci in *rgf1*Δ cells was investigated, where we focused our attention on Rad11p-GFP (Replication protein-A subunit1) (64), Rad54p-GFP (orthologous to *S.cerevisiae* Rad54p) and Rad51p (RecA homologue recombinase). Rad11p removes ssDNA secondary structure and stimulates the assembly of Rad51p nucleofilaments. Rad54p, a member of the SNF2 family of chromatin remodeling DNA-dependent ATPases facilitates chromatin remodeling at the homology search step of HR (65,66). Both are functionally related to Rad52p (18).

In an unperturbed cycle, the number of multiple Rad11p-foci positive cells (n≥2) in the *rgf1*Δ mutant was similar than that of the control cells (Figure 7B). In response to Phl, both Rad11p-GFP and Rad54p-GFP form foci in wild-type and *rgf1*Δ cells, indicating that Rgf1p is not necessary for the initial targeting of the proteins to the DNA lesions (Figure 7B and C). 3 h after treatment, in *rgf1*Δ cells, the percentage of cells containing Rad11p and Rad54p foci remained at nearly the same level seen immediately after the treatment. In contrast, more than half of the wild-type cells had completely lost Rad11p and Rad54p foci at this point (Figure 7B and C, respectively). It is worth mentioning that Rad11p-GFP and Rad54p-GFP cells behaved like wild-type cells with respect to sensitivity to Phl (unpublished observations).

Finally, we analyzed Rad51p loading into DNA by immunofluorescence in wild-type and *rgf1*Δ cells before and after exposure to Phl. Cells with ≥2 Rad51p foci were barely detected before Phl treatment and raised 30 min after treatment in both strains. However, during recovery time the Rad51p foci substantially diminished in the wild-type but persisted in the *rgf1*Δ mutant, probably reflecting a failure to effectively repair DNA damage (Figure 7D).

Future studies defining the interaction of Rgf1p with other DSB repair proteins at Rad52p factories may help to delineate its role in completing DSB repair.

DISCUSSION

Here we report that the exchange factor Rgf1p is involved in the repair of DNA double-strand breaks induced by Phl treatment. In *S. pombe*, the DNA damage checkpoint is activated by Rad3p (ATR homolog), which in turn activates its downstream protein kinase, Chk1p (67). The *rgf1*Δ cells are sensitive to CPT and highly sensitive to Phl, both drugs trigger a strong checkpoint response.

We show that deletion of Rgf1p does not prevent the imposition of the checkpoint induced by Phl, but it does prevent recovery from DNA damage, resulting in permanent activation of Chk1p and permanent arrest of the cells in G2/M. This delay in dephosphorylation of Chk1p indicates that *rgf1*$^+$ deleted cells are defective in re-entry into the cell cycle. However, abrogation of the checkpoint in *rgf1*Δ cells does not rescue the sensitivity to Phl or diminish the number of cells with ≥2 Rad52-YFP after Phl treatment (unpublished observations). Alternatively, disruption of *rgf1*Δ might prevent repair of damaged DNA leading to persistent phosphorylation of Chk1p and failure to reenter the cell cycle. Our data favor the second possibility. In fact, nuclear staining of the *rgf1*Δ null mutant after Phl treatment shows a population of 2C/4C cells with one aberrant nucleus that could have been generated due to the extensive DNA damage (Figure 2D and F). Moreover, the inability of the *rgf1*Δ mutant to efficiently repair fragmented chromosomes (Figure 5A) also supports a role for Rgf1p in DNA repair.

*rgf1*Δ and *rho1-596* cells are only slightly sensitive to acute exposure to IR (Supplementary Figure S1). It is possible that Phl is generating a specific type of replication stress that acute exposure to IR does not. In this sense, as we have shown the *rgf1*Δ cells are also sensitive to CPT, a topoisomerase (Top1p) poison (Figure 1). CPT stabilizes reversible Top1p-DNA covalent complexes, which are often converted to DSBs during DNA replication (47).

What might be the role of Rgf1p in repair? The double-strand break repair process by HR is initiated by nucleolytic trimming of the broken DNA to produce 3′-single stranded overhangs which is rapidly covered by RPA (replication protein A). This RPA–ssDNA complex is recombination inert and needs to be activated by Rad52p, which interacts with the recombinase Rad51p as well as with RPA and facilitates the efficient displacement of RPA on ssDNA by Rad51p (68).

Rad52p is a key protein in HR therefore, one of the most solid pieces of evidence for Rgf1p playing a role in DNA repair comes from the inability of the *rgf1*Δ cells to remove Phl-induced Rad52p-YFP foci, which leads to decreased cell viability. This defect mimics the accumulation of Rad52p-YFP irreparable foci in mutants of the core repair proteins, Rad11p, Rad51p and Rad54p. In contrast, the resolution dynamics of the Rad52-YFP foci in *rgf1*Δ cells was different from that seen in the *mre11* mutant, involved in resection (Figure 7A). Moreover, in the *rgf1*Δ cells and in *rad11*, *rad51*Δ and *rad54*Δ mutants, Rad52p foci form efficiently after Phl, and given that Mre11p and Rad52p localization to damaged sites is mutually exclusive (69), it is very likely that in *rgf1*Δ cells the Mre11p foci would be processed correctly. Altogether, these results suggest that Rgf1p is not involved in processing DNA lesions that precedes the recruitment of core recombination proteins.

As for Rad52p, deletion of *rgf1*$^+$ does not affect recruitment, but accumulates Rad11p-GFP foci, a result that is intriguing (Figure 7B). Contiguous Rad51p–ssDNA filament formation is stimulated in the presence of the ssDNA binding protein replication protein-A (RPA), which removes DNA secondary structure (70). However, if ssDNA is saturated with RPA, Rad51p cannot efficiently remove RPA from ssDNA; therefore, Rad51p–filament formation and DNA strand transfer are inhibited by RPA. This inhibitory effect of RPA is overcome by Rad52p (71–73) that interacts with RPA and Rad51p (58,74–76). In the *rgf1*Δ scenario, Rad52p is accumulated in foci structures for a long time but does not seem to do the job properly. We have discarded that Rad52p stability is being regulated by Rgf1p. Therefore, it is possible that in the absence of Rgf1p or depletion of Rho1p, Rad11p-GFP cannot be disentangled from the ssDNA interfering with Rad52p mediator activity. Alternatively, a blockage of the repair process might also promote the accumulation of Rad11p-GFP. In this sense, Rad54p (Figure 7C) and Rad9p (a component of the

Rad9p–Rad1p–Hus1p-complex) also showed long-lasting foci in the *rgf1*Δ mutant (unpublished observations). Moreover, Rad51p foci follow the same pattern as Rad52p and Rad11p foci in *rgf1*Δ cells. These observations suggest that repair proteins are recruited to the DSB sites, but somehow are unable to conduct the repair reaction and remain there. Thus, the *rgf1*Δ cells also have difficulties dismantling the DNA damage checkpoint (77). Proficient formation of repair protein foci and their retention at DSBs in the *rgf1*Δ mutant suggest that *rgf1*Δ cells have a defect in the pathway parallel to repair protein recruitment.

Finally, retention of Rad11p-GFP, Rad54p-GFP and Rad51p foci during recovery from DNA damage could satisfactorily explain the sustained checkpoint response in *rgf1*Δ cells. RPA is necessary for recruiting a number of checkpoint and HR proteins. RPA recruits the Rad3p checkpoint kinase, which phosphorylates and activates the checkpoint kinase Chk1p sites. This event requires the Rad9p–Rad1p–Hus1p checkpoint clamp and Crb2p mediator proteins. Interestingly, RPA also recruits the 9-1-1-complex (DNA damage checkpoint clamp) to the DNA repair sites (22). Therefore, in cells deleted for Rgf1p the mediator activity of Crb2p and that of the checkpoint clamp might account for inhibition of Cdc25p by Chk1p which delays the onset of mitosis.

Rgf1p constantly moves in and out of the nucleus in an unperturbed cell cycle (41). According to the role proposed here, Rgf1p must be present in the nucleus of the cells treated with Phl. This was indeed the case, although Rgf1p was not concentrated in foci like the classical repair proteins, the addition of Leptomycin B after Phl treatment, a drug that blocks nuclear exit, trapped the protein in the nucleus (not shown). Interestingly, Rgf1p-GFP was re-localized to the SPBs after Phl treatment (not shown). It is worth mentioning that persistent DSBs arising in S/G2 can be recruited to the Sad1p-Unc-84-related (SUN) domain protein Sad1p, leading to their association with the oscillating SPB (27).

Here, we propose a new role for Rgf1p and the Rho1p signaling pathway in DSB repair in fission yeast. Given that Rho-GEFs and Rho GTPases show conserved functions it will be of general interest to determine whether their function in surviving DNA damage is also conserved in higher eukaryotes.

SUPPLEMENTARY DATA

Supplementary Data are available at NAR Online.

ACKNOWLEDGEMENTS

We wish to thank P. Sunnerhagen, S. Gasser, P. Meister, P. Perez, J. Cansado, J.C. Ribas, A. Bueno, K. Komatsu, T. Nakamura, T. Nakagawa, R. McFarlane, T. C. Humphrey, S. Forsburg and S. Moreno for providing strains and plasmids. R. Barrios is acknowledged for technical help. C. Martin-Castellanos and L. Bustamante are acknowledged for their help with CHEF analysis and A. Clemente-Blanco for critical comments on the manuscript. The English text was revised by E. Keck. E. Manjón and T. Edreira were supported by a contract from the Junta de Castilla y León co-financed by the Fondo Social Europeo and S. Muñoz acknowledges the support from the JAE-PreDoc fellowship provided by the CSIC, Spain.

FUNDING

CICYT, Spain [BFU2011-24683/BMC]; Junta de Castilla y León [SA073U14]. Funding for open access charge: MINECO.
Conflict of interest statement. None declared.

REFERENCES

1. Cook,D.R., Rossman,K.L. and Der,C.J. (2014) Rho guanine nucleotide exchange factors: regulators of Rho GTPase activity in development and disease. *Oncogene*, **33**, 4021–4035.
2. Hall,A. (2012) Rho family GTPases. *Biochem. Soc. Trans.*, **40**, 1378–1382.
3. Ridley,A.J. (2015) Rho GTPase signalling in cell migration. *Curr. Opin. Cell Biol.*, **36**, 103–112.
4. Rossman,K.L., Channing,J.D. and Sondek,J. (2005a) GEF means go: turning on Rho GTPases with guanine nucleotide-exchange factors. *Nat. Rev. Mol. Cell Biol.*, **6**, 167–180.
5. Rajakyla,E.K. and Vartiainen,M.K. (2014) Rho, nuclear actin, and actin-binding proteins in the regulation of transcription and gene expression.*Small GTPases*, **5**, e27539.
6. Weston,L., Coutts,A.S. and La Thangue,N.B. (2012) Actin nucleators in the nucleus: an emerging theme. *J. Cell Sci.*, **125**, 3519–3527.
7. Mamouni,K., Cristini,A., Guirouilh-Barbat,J., Monferran,S., Lemarie,A., Faye,J.C., Lopez,B.S., Favre,G. and Sordet,O. (2014) RhoB promotes gammaH2AX dephosphorylation and DNA double-strand break repair. *Mol. Cell. Biol.*, **34**, 3144–3155.
8. Wang,H., Zhang,X., Teng,L. and Legerski,R.J. (2015) DNA damage checkpoint recovery and cancer development. *Exp. Cell Res.*, **334**, 350–358.
9. Dubash,A.D., Guilluy,C., Srougi,M.C., Boulter,E., Burridge,K. and Garcia-Mata,R. (2011) The small GTPase RhoA localizes to the nucleus and is activated by Net1 and DNA damage signals. *PLoS One*, **6**, e17380.
10. Guerra,L., Carr,H.S., Richter-Dahlfors,A., Masucci,M.G., Thelestam,M., Frost,J.A. and Frisan,T. (2008) A bacterial cytotoxin identifies the RhoA exchange factor Net1 as a key effector in the response to DNA damage. *PLoS One*, **3**, e2254.
11. Srougi,M.C. and Burridge,K. (2011) The nuclear guanine nucleotide exchange factors Ect2 and Net1 regulate RhoB-mediated cell death after DNA damage. *PLoS One*, **6**, e17108.
12. Jackson,S.P. and Bartek,J. (2009) The DNA-damage response in human biology and disease. *Nature*, **461**, 1071–1078.
13. Bartek,J. and Lukas,J. (2007) DNA damage checkpoints: from initiation to recovery or adaptation. *Curr. Opin. Cell Biol.*, **19**, 238–245.
14. Ciccia,A. and Elledge,S.J. (2010) The DNA damage response: making it safe to play with knives. *Mol. Cell*, **40**, 179–204.
15. Finn,K., Lowndes,N.F. and Grenon,M. (2012) Eukaryotic DNA damage checkpoint activation in response to double-strand breaks. *Cell. Mol. Life Sci.*, **69**, 1447–1473.
16. Chapman,J.R., Taylor,M.R. and Boulton,S.J. (2012) Playing the end game: DNA double-strand break repair pathway choice. *Mol. Cell*, **47**, 497–510.
17. Symington,L.S. (2016) Mechanism and regulation of DNA end resection in eukaryotes. *Crit. Rev. Biochem. Mol. Biol.*, **51**, 195–212.
18. Raji,H. and Hartsuiker,E. (2006) Double-strand break repair and homologous recombination in Schizosaccharomyces pombe. *Yeast*, **23**, 963–976.
19. Meister,P., Poidevin,M., Francesconi,S., Tratner,I., Zarzov,P. and Baldacci,G. (2003) Nuclear factories for signalling and repairing DNA double strand breaks in living fission yeast. *Nucleic Acids Res.*, **31**, 5064–5073.
20. Lisby,M., Mortensen,U.H. and Rothstein,R. (2003) Colocalization of multiple DNA double-strand breaks at a single Rad52 repair centre. *Nat. Cell Biol.*, **5**, 572–577.

21. Blaikley,E.J., Tinline-Purvis,H., Kasparek,T.R., Marguerat,S., Sarkar,S., Hulme,L., Hussey,S., Wee,B.Y., Deegan,R.S., Walker,C.A. *et al.* (2014) The DNA damage checkpoint pathway promotes extensive resection and nucleotide synthesis to facilitate homologous recombination repair and genome stability in fission yeast. *Nucleic Acids Res.*, **42**, 5644–5656.
22. Langerak,P. and Russell,P. (2011) Regulatory networks integrating cell cycle control with DNA damage checkpoints and double-strand break repair. *Philos. Trans. R. Soc. Lond. B Biol. Sci.*, **366**, 3562–3571.
23. Agmon,N., Liefshitz,B., Zimmer,C., Fabre,E. and Kupiec,M. (2013) Effect of nuclear architecture on the efficiency of double-strand break repair. *Nat. Cell Biol.*, **15**, 694–699.
24. Mine-Hattab,J. and Rothstein,R. (2012) Increased chromosome mobility facilitates homology search during recombination. *Nat. Cell Biol.*, **14**, 510–517.
25. Seeber,A., Dion,V. and Gasser,S.M. (2013) Checkpoint kinases and the INO80 nucleosome remodeling complex enhance global chromatin mobility in response to DNA damage. *Genes Dev.*, **27**, 1999–2008.
26. Shimada,K., Filipuzzi,I., Stahl,M., Helliwell,S.B., Studer,C., Hoepfner,D., Seeber,A., Loewith,R., Movva,N.R. and Gasser,S.M. (2013) TORC2 signaling pathway guarantees genome stability in the face of DNA strand breaks. *Mol. Cell*, **51**, 829–839.
27. Swartz,R.K., Rodriguez,E.C. and King,M.C. (2014) A role for nuclear envelope-bridging complexes in homology-directed repair. *Mol. Biol. Cell*, **25**, 2461–2471.
28. Nakano,K., Arai,R. and Mabuchi,I. (1997) The small GTP binding protein Rho1 is a multifunctional protein that regulates actin localization, cell polarity, and septum formation in the fission yeast *Schizosaccharomyces pombe*. *Genes Cells*, **2**, 679–694.
29. Arellano,M., Duran,A. and Perez,P. (1997) Localization of the *Schizosaccharomyces pombe* Rho1 GTPase and its involvement in the organization of the actin cytoskeleton. *J. Cell. Sci.*, **110**, 2547–2555.
30. García,P., Tajadura,V., García,I. and Sánchez,Y. (2006b) Role of Rho GTPses and Rho-GEFs in the regulation of cell shape and integrity in fission yeast. *Yeast*, **23**, 1031–1043.
31. García,P., García,I., Marcos,F., Ruiz de Garibay,G. and Sánchez,Y. (2009b) Fission yeast Rgf2p is a Rho1p guanine nucleotide exchange factor required for spore wall maturation and for the maintenance of cell integrity in the absence of Rgf1p. *Genetics*, **181**, 1321–1334.
32. García,P., Tajadura,V., García,I. and Sánchez,Y. (2006a) Rgf1p is a specific Rho1-GEF that coordinates cell polarization with cell wall biogenesis in fission yeast. *Mol. Biol. Cell*, **17**, 1620–1631.
33. Morrell-Falvey,J.L., Ren,L., Feoktistova,A., Haese,G.D. and Gould,K.L. (2005) Cell wall remodeling at the fission yeast cell division site requires the Rho-GEF Rgf3p. *J. Cell Sci.*, **118**, 5563–5573.
34. Mutoh,T., Nakano,K. and Mabuchi,I. (2005) Rho1-GEFs Rgf1 and Rgf2 re involved in formation of cell wall and septum, while Rgf3 is involved in cytokinesis in fission yeast. *Genes Cells*, **10**, 1189–1202.
35. Tajadura,V., Garcia,B., Garcia,I., Garcia,P. and Sanchez,Y. (2004) *Schizosaccharomyces pombe* Rgf3p is a specific Rho1 GEF that regulates cell wall β-glucan biosynthesis through the GTPase Rho1p. *J. Cell Sci.*, **117**, 6163–6174.
36. Perez,P. and Rincón,S.A. (2010) Rho GTPases: regulation of cell polarity and growth in yeasts. *Biochem. J.*, **426**, 243–253.
37. Garcia,P., Tajadura,V. and Sanchez,Y. (2009a) The Rho1p exchange factor Rgf1p signals upstream from the Pmk1 mitogen-activated protein kinase pathway in fission yeast. *Mol. Biol. Cell* , **20**, 721–731.
38. Ma,Y., Kuno,T., Kita,A., Asayama,Y. and Sugiura,R. (2006) Rho2 is a target of the farnesiltransferase Cpp1 and acts upstream of Pmk1 mitogen-activated protein kinase signaling in fission yeast. *Mol. Biol. Cell*, **17**, 5028–5037.
39. Sanchez-Mir,L., Soto,T., Franco,A., Madrid,M., Viana,R.A., Vicente,J., Gacto,M., Perez,P. and Cansado,J. (2014) Rho1 GTPase and PKC ortholog Pck1 are upstream activators of the cell integrity MAPK pathway in fission yeast. *PLoS One*, **9**, e88020.
40. Viana,R.A., Pinar,M., Soto,T., Coll,P.M., Cansado,J. and Perez,P. (2013) Negative functional interaction between cell integrity MAPK pathway and Rho1 GTPase in fission yeast. *Genetics*, **195**, 421–432.
41. Munoz,S., Manjon,E., Garcia,P., Sunnerhagen,P. and Sanchez,Y. (2014a) The checkpoint-dependent nuclear accumulation of Rho1p exchange factor Rgf1p is important for tolerance to chronic replication stress. *Mol. Biol. Cell*, **25**, 1137–1150.
42. Moreno,S., Klar,A. and Nurse,P. (1991) Molecular genetic analysis of fission yeast *Schizosaccharomyces pombe*. *Meth. Enzymol.*, **194**, 795–823.
43. Jaendling,A., Ramayah,S., Pryce,D.W. and McFarlane,R.J. (2008) Functional characterisation of the Schizosaccharomyces pombe homologue of the leukaemia-associated translocation breakpoint binding protein translin and its binding partner, TRAX. *Biochim. Biophys. Acta*, **1783**, 203–213.
44. Takeda,J., Uematsu,N., Shiraishi,S., Toyoshima,M., Matsumoto,T. and Niwa,O. (2008) Radiation induction of delayed recombination in Schizosaccharomyces pombe. *DNA Repair (Amst)*, **7**, 1250–1261.
45. Hall,B.M., Ma,C.X., Liang,P. and Singh,K.K. (2009) Fluctuation analysis CalculatOR: a web tool for the determination of mutation rate using Luria-Delbruck fluctuation analysis. *Bioinformatics*, **25**, 1564–1565.
46. Caspari,T., Murray,J.M. and Carr,A.M. (2002) Cdc2-cyclin B kinase activity links Crb2 and Rqh1-topoisomerase III. *Genes Dev.*, **16**, 1195–1208.
47. Pommier,Y. (2006) Topoisomerase I inhibitors: camptothecins and beyond. *Nat. Rev. Cancer*, **6**, 789–802.
48. Chen,J. and Stubbe,J. (2004) Bleomycins: new methods will allow reinvestigation of old issues. *Curr. Opin. Chem. Biol.*, **8**, 175–181.
49. Levin,J.D. and Demple,B. (1996) In vitro detection of endonuclease IV-specific DNA damage formed by bleomycin in vivo. *Nucleic Acids Res.*, **24**, 885–889.
50. Chang,M., Bellaoui,M., Boone,C. and Brown,G.W. (2002) A genome-wide screen for methyl methanesulfonate-sensitive mutants reveals genes required for S phase progression in the presence of DNA damage. *Proc. Natl. Acad. Sci. U.S.A.*, **99**, 16934–16939.
51. Wan,S., Capasso,H. and Walworth,N.C. (1999) The topoisomerase I poison camptothecin generates a Chk1-dependent DNA damage checkpoint signal in fission yeast. *Yeast*, **15**, 821–828.
52. Enserink,J.M., Smolka,M.B., Zhou,H. and Kolodner,R.D. (2006) Checkpoint proteins control morphogenetic events during DNA replication stress in Saccharomyces cerevisiae. *J. Cell Biol.*, **175**, 729–741.
53. Smolka,M.B., Chen,S.H., Maddox,P.S., Enserink,J.M., Albuquerque,C.P., Wei,X.X., Desai,A., Kolodner,R.D. and Zhou,H. (2006) An FHA domain-mediated protein interaction network of Rad53 reveals its role in polarized cell growth. *J. Cell Biol.*, **175**, 743–753.
54. Yoshida,S., Bartolini,S. and Pellman,D. (2009) Mechanisms for concentrating Rho1 during cytokinesis. *Genes Dev.* , **23**, 810–823.
55. Yoshida,S., Kono,K., Lowery,D., Bartolini,S., Yaffe,M., Ohya,Y. and Pellman,D. (2006) Polo-like kinase Cdc5 controls the local activation of Rho1 to promote cytokinesis. *Science*, **313**, 108–111.
56. Brondello,J.M., Boddy,M.N., Furnari,B. and Russell,P. (1999) Basis for the checkpoint signal specificity that regulates Chk1 and Cds1 protein kinases. *Mol. Cell. Biol.*, **19**, 4262–4269.
57. Kim,W.J., Lee,S., Park,M.S., Jang,Y.K., Kim,J.B. and Park,S.D. (2000) Rad22 protein, a rad52 homologue in Schizosaccharomyces pombe, binds to DNA double-strand breaks. *J. Biol. Chem.*, **275**, 35607–35611.
58. Saito,Y., Takeda,J., Okada,M., Kobayashi,J., Kato,A., Hirota,K., Taoka,M., Matsumoto,T., Komatsu,K. and Isobe,T. (2013) The proteasome factor Bag101 binds to Rad22 and suppresses homologous recombination. *Sci. Rep.*, **3**, 2022.
59. Ferreira,M.G. and Cooper,J.P. (2004) Two modes of DNA double-strand break repair are reciprocally regulated through the fission yeast cell cycle. *Genes Dev.*, **18**, 2249–2254.
60. Doe,C.L., Osman,F., Dixon,J. and Whitby,M.C. (2004) DNA repair by a Rad22-Mus81-dependent pathway that is independent of Rhp51. *Nucleic Acids Res.*, **32**, 5570–5581.
61. Manolis,K.G., Nimmo,E.R., Hartsuiker,E., Carr,A.M., Jeggo,P.A. and Allshire,R.C. (2001) Novel functional requirements for non-homologous DNA end joining in Schizosaccharomyces pombe. *EMBO J.*, **20**, 210–221.
62. Pierce,A.J., Hu,P., Han,M., Ellis,N. and Jasin,M. (2001) Ku DNA end-binding protein modulates homologous repair of double-strand breaks in mammalian cells. *Genes Dev.*, **15**, 3237–3242.
63. Zhang,Y., Hefferin,M.L., Chen,L., Shim,E.Y., Tseng,H.M., Kwon,Y., Sung,P., Lee,S.E. and Tomkinson,A.E. (2007) Role of Dnl4-Lif1 in nonhomologous end-joining repair complex assembly and

suppression of homologous recombination. *Nat. Struct. Mol. Biol.*, **14**, 639–646.
64. Parker,A.E., Clyne,R.K., Carr,A.M. and Kelly,T.J. (1997) The Schizosaccharomyces pombe rad11+ gene encodes the large subunit of replication protein A. *Mol. Cell. Biol.*, **17**, 2381–2390.
65. Alexeev,A., Mazin,A. and Kowalczykowski,S.C. (2003) Rad54 protein possesses chromatin-remodeling activity stimulated by the Rad51-ssDNA nucleoprotein filament. *Nat. Struct. Biol.*, **10**, 182–186.
66. Wolner,B. and Peterson,C.L. (2005) ATP-dependent and ATP-independent roles for the Rad54 chromatin remodeling enzyme during recombinational repair of a DNA double strand break. *J. Biol. Chem.*, **280**, 10855–10860.
67. Carr,A.M. (2002) DNA structure dependent checkpoints as regulators of DNA repair. *DNA Repair (Amst)*, **1**, 983–994.
68. Lisby,M. and Rothstein,R. (2009) Choreography of recombination proteins during the DNA damage response. *DNA Repair (Amst)*, **8**, 1068–1076.
69. Lisby,M., Barlow,J.H., Burgess,R.C. and Rothstein,R. (2004) Choreography of the DNA damage response: spatiotemporal relationships among checkpoint and repair proteins. *Cell*, **118**, 699–713.
70. Sugiyama,T., Zaitseva,E.M. and Kowalczykowski,S.C. (1997) A single-stranded DNA-binding protein is needed for efficient presynaptic complex formation by the Saccharomyces cerevisiae Rad51 protein. *J. Biol. Chem.*, **272**, 7940–7945.
71. New,J.H., Sugiyama,T., Zaitseva,E. and Kowalczykowski,S.C. (1998) Rad52 protein stimulates DNA strand exchange by Rad51 and replication protein A. *Nature*, **391**, 407–410.
72. Shinohara,A. and Ogawa,T. (1998) Stimulation by Rad52 of yeast Rad51-mediated recombination. *Nature*, **391**, 404–407.
73. Sung,P. (1997) Function of yeast Rad52 protein as a mediator between replication protein A and the Rad51 recombinase. *J. Biol. Chem.*, **272**, 28194–28197.
74. Hays,S.L., Firmenich,A.A., Massey,P., Banerjee,R. and Berg,P. (1998) Studies of the interaction between Rad52 protein and the yeast single-stranded DNA binding protein RPA. *Mol. Cell. Biol.*, **18**, 4400–4406.
75. Song,B. and Sung,P. (2000) Functional interactions among yeast Rad51 recombinase, Rad52 mediator, and replication protein A in DNA strand exchange. *J. Biol. Chem.*, **275**, 15895–15904.
76. Tsutsui,Y., Khasanov,F.K., Shinagawa,H., Iwasaki,H. and Bashkirov,V.I. (2001) Multiple interactions among the components of the recombinational DNA repair system in Schizosaccharomyces pombe. *Genetics*, **159**, 91–105.
77. Shaltiel,I.A., Krenning,L., Bruinsma,W. and Medema,R.H. (2015) The same, only different - DNA damage checkpoints and their reversal throughout the cell cycle. *J. Cell Sci.*, **128**, 607–620.